IEEE Access
Multidisciplinary | Rapid Review | Open Access Journal

SPECIAL SECTION ON ANTENNA AND PROPAGATION FOR 5G AND BEYOND

Received October 20, 2019, accepted October 28, 2019, date of publication October 31, 2019, date of current version November 13, 2019.

Digital Object Identifier 10.1109/ACCESS.2019.2950660

Realization of a Tapered Slot Array as Both Decoupling and Radiating Structure for 4G/5G Wireless Devices

MUHAMMAD IKRAM, (Student Member, IEEE), NGHIA NGUYEN-TRONG, (Member, IEEE), AND AMIN M. ABBOSH, (Senior Member, IEEE)

School of Information Technology and Electrical Engineering, The University of Queensland (UQ), Brisbane, QLD 4072, Australia

Corresponding author: Muhammad Ikram (m.ikram@uq.edu.au)

This work was supported by the Australian Research Council under ARC Grant LP160100917.

ABSTRACT As a combination of microwave Multiple-Input Multiple-Output (MIMO) antenna system and mm-wave antenna array, an integrated design is proposed to provide multi-band, high port isolation, and high gain antenna solution for 4G/5G wireless devices. In this work, an array of tapered slots is used as a decoupling structure at microwave frequency and as an antenna array at mm-wave frequency. The proposed geometry consists of a dual-band monopole MIMO antenna system operating at 4G (2.6 GHz) and 5G (3.5 GHz) sub-6 GHz bands. The wideband port isolation of more than 25 dB is achieved by introducing a tapered slot array structure. One of the key design features is the utilization of these slots as an antenna array with a peak realized gain of 15 dBi at 28 GHz, making this array dual-functional, thus more feasible for compact 4G/5G handheld devices. The proposed design is printed on an RO-5880 substrate with an overall size of 70 mm $\times$ 50 mm $\times$ 0.51 mm. The measured -10-dB impedance matching bandwidth covers two sub-6 GHz bands (from 2.45 GHz to 2.85 GHz and from 3.18 GHz to 3.68 GHz), and the wide mm-wave band from 25 GHz to 30 GHz.

INDEX TERMS Decoupling, MIMO, tapered slot antenna array, 4G/5G.

I. INTRODUCTION

Compact, integrated, and multi-functional antennas have recently been investigated intensively and are highly desirable for various applications in wireless communication systems, especially in handheld devices where size constraint persists. In addition, owing to the rapid demand for high data rates from those devices, MIMO and mm-wave technologies have been proposed as enabling technologies for future wireless communication systems [1], [2]. However, there are serious challenges, such as size constraints and high number of antenna elements at low frequency bands in MIMO technology and path loss, penetration, and high gain antenna arrays in mm-wave technology. To solve those challenges, integrated antenna solutions that can be used as a MIMO antenna system at low frequency band and a high gain antenna array at mm-wave bands are required [3]–[5].

Several integrated antenna solutions were reported for mobile phones, WiFi, and wireless routers applications [4]–[16]. However, some of the presented designs cover only low frequency 4G/5G bands [6]–[11] and hence, are unable to support mm-wave bands. The remaining were presented for both microwave (4G, WLAN) and mm-wave (5G) bands [4], [5], [12]–[16]. Nevertheless, all those designs were presented without MIMO configuration at microwave bands and had relatively low gain at mm-wave bands which is less suitable for 5G applications.

Recently, slot antennas have gained high attention due to its dual-functional characteristics [3], [17]. The slot was presented in [18], [19] as both an isolation enhancement structure and a connected antenna array, whereas in [3], it was used as a frequency-reconfigurable radiator at microwave band and as a connected array at mm-wave band. Additionally, a tapered slot antenna was also reported in [20] as an isolation enhancement structure at microwave band and as an end-fire mm-wave antenna. Due to bidirectional radiation patterns or using single antenna element at mm-wave bands, those aforementioned designs had relatively low gain values. It is also noted that the design in [20] was not intended for mobile devices due to the presence of a circular aperture.

The associate editor coordinating the review of this manuscript and approving it for publication was Hassan Tariq Chattha.

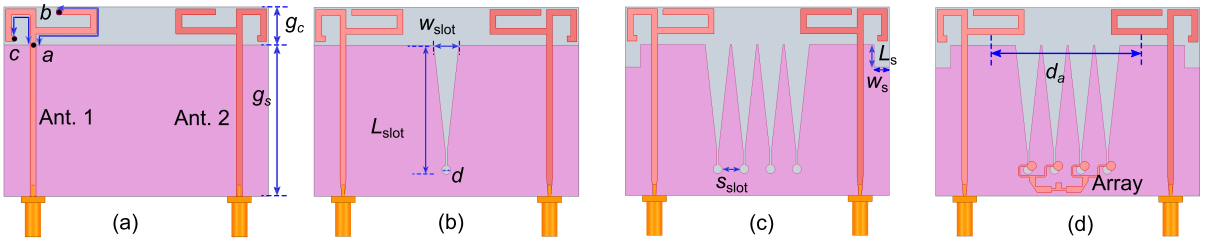

FIGURE 1. Realization of the proposed design. Monopole MIMO antenna design (a) without, (b) with single, and (c) with array of tapered slots, and (d) final design.

This work presents a concept of dual-band monopole MIMO antenna integrated with a tapered slot antenna array (TSAA) for 4G/5G mobile devices. The proposed structure exploits the geometry of 2-element monopole MIMO design, which operates at 2.6 GHz (from 2.45 GHz to 2.85 GHz) and 3.5 GHz (from 3.18 GHz to 3.68 GHz). Due to the small inter-element spacing ($<\lambda_o/2$ at 2.6 GHz, λ_o is a free space wavelength) and sharing the same ground plane, an efficient decoupling structure is required. This is achieved by exploiting the TSAA, which also works as an end-fire antenna array at 28 GHz band with a peak realized gain of 15 dBi, thus making the TSAA a dual-functional structure. The TSAA provides both high isolation at microwave band and high gain at mm-wave band. Overall, more than 25-dB isolation is achieved for a wideband from 2.45 GHz to 3.68 GHz, which is a substantial improvement compared to the reported designs [17], [18], [20], [21].

II. CONFIGURATIONS OF MIMO ANTENNA SYSTEM AND TAPERED SLOT ANTENNA ARRAY

The proposed structure starts with a 2-element meandered monopole MIMO antenna system as shown in Fig. 1(a). The aim is to present a highly isolated MIMO antenna design with omnidirectional radiation patterns [22]–[24] at two targeted operating bands, i.e. 2.6 GHz and 3.5 GHz since these two bands are common for 4G and 5G applications. Many techniques have been proposed in the literature to improve the isolation between closely spaced antennas [20], [21], [25]–[27]. Here, defected ground structure (DGS) based on a tapered slot is exploited. However, instead of using a single tapered slot [20], [28], an array of tapered slots is realized (see Fig. 1(d)) in order to achieve wideband isolation at microwave band and high gain at mm-wave band.

The geometry of the final proposed design with its fabricated prototype is shown in Fig. 2. This proposed design is modeled on a Rogers RT/duroid 5880 substrate ($\tan\delta = 0.0009$ at 10 GHz, $\epsilon_r = 2.2$) with the total size of 70 mm × 50 mm × 0.51 mm. Two monopoles and feeding structure are etched on the top layer, while a ground plane with an array of tapered slots are etched in the bottom layer of the substrate. The size of the ground plane is critical since it can affect the performance of the monopole. However, the monopole and the size of the ground plane which in conjunction with the substrate can be tailored to suit different

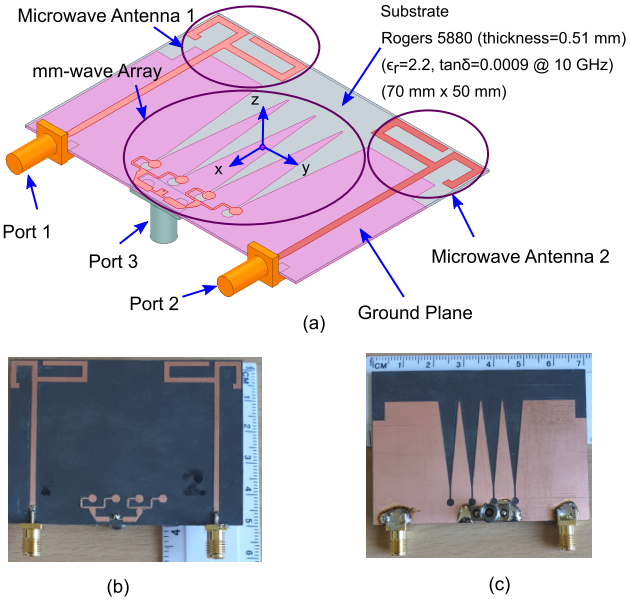

FIGURE 2. The geometry of the proposed design. (a) Isometric view and photographs of fabricated prototype (b) front view and (c) back view.

applications, i.e. smartphones, WiFi devices or other handheld devices. For simulations and measurements, a simple 50-Ω SMA connector is utilized for microwave frequency ports (Port 1 and Port 2) and a 50-Ω RF coaxial precision connector (DC-40 GHz) is used for mm-wave port (Port 3).

III. DESIGN AND OPTIMIZATION

The simulations and optimization of the proposed work are carried out using ANSYS High Frequency Structure Simulator (HFSS). The design of single tapered slot antenna is well known and can be found in [20], [28]–[30]. Here, we focus on the array configuration and the integrated structure performance. All optimized parameters are as follows: $L_{a-b} = 38$, $L_{a-c} = 19.2$, $g_s = 40$, $g_c = 10$, $d_a = 40$, $L_s = 6$, $w_s = 4$, $d = 2.4$, $L_{\text{slot}} = 34$, $W_{\text{slot}} = 6.7$, $d_{\text{stub}} = 3.40$, $S_{\text{stub}} = 3.40$, and $d_f = 6.53$. all values are in millimeter (mm).

A. DUAL-BAND MIMO ANTENNA DESIGN

Fig. 3(a) shows the simulated performance of a dual-band monopole MIMO antenna design shown in Fig. 1(a). Each monopole has two main radiating arms having lengths of

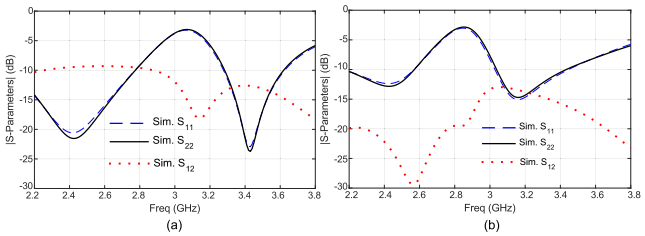

FIGURE 3. S-parameters (a) before and (b) after adding a single tapered slot.

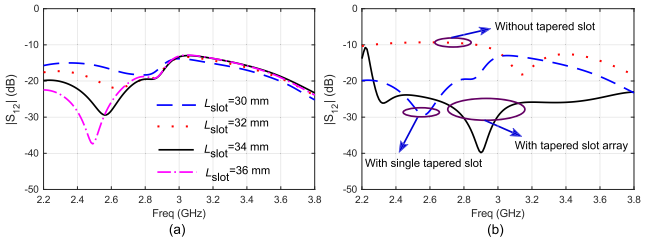

FIGURE 4. (a) $|S_{12}|$ for different values of slot length and (b) $|S_{12}|$ for three different cases.

L_{a-b} and L_{a-c}. These lengths are optimized to cover 2.6 GHz and 3.5 GHz bands with satisfactory impedance matching bandwidths. The simulated S-parameters are also shown in Fig. 3(a). It can be seen that the antenna covers two bands from 2.1 GHz to 2.8 GHz and from 3.3 GHz to 3.6 GHz.

Due to the small inter-element spacing ($<\lambda_o/2$ at 2.6 GHz) and sharing the same ground plane, a low isolation of $|S_{12}| =$ 9 dB at 2.6 GHz and $|S_{12}| = 12$ dB at 3.5 GHz is observed between monopoles. The mutual coupling can also be verified from current distributions as shown in Fig. 5(a). When Port 1 (Ant. 1) is excited and Port 2 (Ant. 2) is terminated with 50 Ω matched load, large surface current can be seen on Ant. 2 showing strong mutual coupling between monopoles.

B. DECOUPLING STRUCTURE BASED ON DEFECTED GROUND STRUCTURE (DGS)

A decoupling technique based on a defected ground structure (DGS) is used to improve the isolation [18], [21]. First, a single tapered slot is etched in the ground plane. The geometry of the tapered slot is shown in Fig. 1(b). The length of the slot (L_{slot}) is a critical parameter which should be around $\lambda_o/4$ at 2.6 GHz since λ_o was defined above at that frequency. It can be noticed that the length of the slot is similar to the length of an open-ended slot antenna which works here as a band reject filter and improves the isolation [28] at the targeted frequency band as shown in Fig. 3(b). The targeted band can be achieved by changing the length (L_{slot}) of the tapered slot as shown in Fig. 4(a). Whereas, the bandwidth of the targeted band can be adjusted by optimizing the width (W_{slot}) and diameter of the circular stub (d) of the tapered slot. Nevertheless, this structure is narrow band and provides band-stop notch that corresponds to high isolation only at a specific frequency band. This can be clearly seen from Fig. 3(b) and Fig. 4(a). It only improves the isolation at 2.6 GHz band and no improvement is observed at 3.5 GHz band.

In the proposed design, instead of the single tapered slot, an array of tapered slots (see Fig. 1(c) and Fig. 6(a)) is used. This structure provides higher isolation in a large bandwidth since it can be considered as a higher-order band reject filter. The comparison of $|S_{12}|$ in three different cases: without slot, with a single slot, and with an array of slots is shown in Fig. 4(b). It is clear from the results that an array of tapered slots provides larger and wider band isolations. In comparison with the other decoupling mechanisms such as [18], [21], [27], [28], the proposed structure is also simple but yields much wider band decoupling characteristic in a tradeoff with structure size.

As discussed previously, the array of tapered slots is also utilized as an antenna array for 5G mm-wave band (discussed in Section III-C) by maintaining the high isolation at microwave bands. Therefore, a tradeoff is required between the number of tapered slots and spacing (S_{slot}) between slots depending on the space between monopoles and required gain at mm-wave band. Here, 4 tapered slots are used so that they can be placed conveniently between monopoles with high gain and beam scanning capabilities. The spacing (S_{slot}) between array of slots is kept 4.6 mm which is less than $\lambda_o/2$ at 28 GHz to avoid grating lobes. The length (L_{slot}) and width (W_{slot}) of the tapered slot are optimized to achieve high isolation in a wide bandwidth. Once satisfactory isolation is achieved, their values are kept constant as $L_{\text{slot}} = 34$ mm and $W_{\text{slot}} = 6.7$ mm. The current distributions are shown in Fig. 5(b), which further verifies the significant improvement (reduction in coupling current) in the isolation.

Due to etching of the array of tapered slots in the ground plane, the impedance matching at 3.5 GHz becomes slightly worse. Therefore, a small rectangular slot on the edge of the ground plane (see Fig. 1(c)) is etched in the ground plane which generates an extra inductance to improve the matching at 3.5 GHz. The length L_s and width w_s of the slot are optimized such that the $|S_{11}|$ are about -15 dB at 3.5 GHz.

C. TAPERED SLOT ANTENNA ARRAY (TSAA)

In this section, the tapered slot antenna array (TSAA), which is designed in Section III-B, is fed from a power divider to operate at 28 GHz as a high gain end-fire antenna array. Thus, the TSAA has dual features: working as a decoupling structure at microwave bands and operating as an antenna array at mm-wave band.

The geometry of the TSAA including four microstrip feeding lines is shown in Fig. 6(a). Each feeding line consists of a 100 Ω transmission line which is terminated with a circular stub to improve the impedance matching. The diameter d of the stub is around $\lambda_g/4$ at 28 GHz. The parameters d_{stub}, S_{stub}, and d_f are optimized to cover a wide mm-wave band with satisfactory impedance matching. The simulated performance of the TSAA is shown in Fig. 6. The stable realized gain (changes from 16 dBi to 14 dBi) in the whole band from 25 GHz to 31 GHz confirms a wide-band characteristic. The

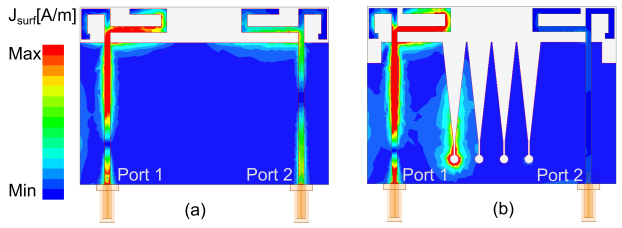

FIGURE 5. Current distributions at 2.6 GHz. (a) before and (b) after adding tapered slot array.

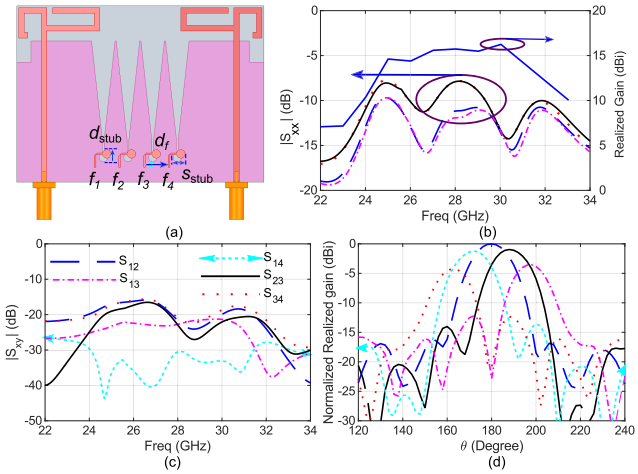

FIGURE 6. Array performance. (a) Geometry, (b) $|S_{xx}|$ and realized gain, (c) $|S_{xy}|$, and (d) beam scanning characteristics.

isolation between adjacent feeding ports is more than 16 dB as shown in Fig. 6(c).

The beam scanning performance of the array is verified in simulation by keeping the magnitude constant and varying the phase (assuming phase shifters for real design) at each port. The results are shown in Fig. 6(d). It can be seen that the proposed TSAA can scan the beam from -18^o to $+18^o$ with the loss of about 3 dB gain.

Finally, a compact 1×4 power divider with the same magnitude and equal phase is designed to test and validate the proposed array (Fig. 1(d)). The tapering is realized to make the power divider compact and wide-band [3]. Due to the high isolation of more than 30 dB between low (Port 1 or Port 2) and high (Port 3) frequency ports, the performance of monopoles remains the same after adding the feeding network.

D. STEP-BY-STEP DESIGN PROCEDURE

A step-by-step procedure is summarized below to demonstrate the proposed concept in a generic way.

- Select the targeted frequencies at microwave band, i.e. 2.6 GHz and 3.5 GHz.
- Choose the initial lengths of monopole, i.e. L_{a-b} and L_{a-c} by $\lambda_o/4$ at 2.6 GHz and 3.5 GHz, respectively.
- Optimize L_{a-b}, L_{a-c}, and their locations to achieve satisfactory results.

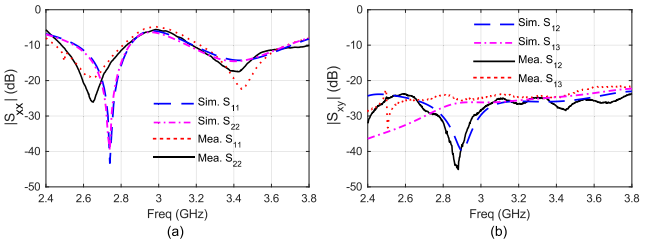

FIGURE 7. The simulated and measured S-parameters of the proposed design for Ant. 1 and Ant. 2. (a) $|S_{xx}|$ and $|S_{xy}|$.

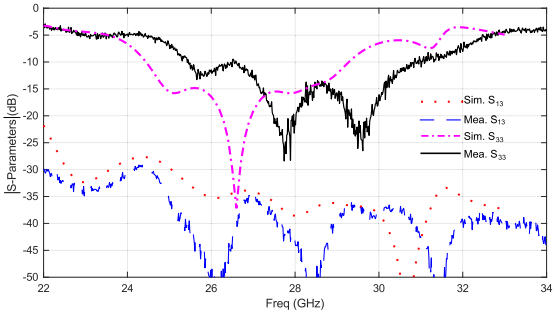

FIGURE 8. The simulated and measured S-parameters of the proposed design for 5G Array.

- Form the MIMO configuration of the monopole antenna.
- Add and optimize the TSAA to improve the isolation between MIMO antennas. Since this tapered slot array will also be used for 5G mm-wave band, its geometry must be designed based on the design procedure demonstrated in [20], [28]–[30]. The spacing between each tapered slot must be less than $\lambda_o/2$ at 28 GHz.
- Add a feeding network to excite the TSAA.
- Optimize the final structure to satisfy the requirements of microwave MIMO antenna and mm-wave array design.

IV. RESULTS, DISCUSSIONS, AND COMPARISONS

In this section, simulated and measured results are compared and discussed. A prototype was fabricated and tested to validate the proposed design (Fig. 2).

The simulated and measured reflection coefficients for low frequency 4G/5G bands are shown in Fig. 7(a). Both Ant. 1 and Ant. 2 operate at 2.6 GHz and 3.5 GHz with -10 dB impedance matching bandwidths of 400 MHz and 500 MHz, respectively. The measured isolation between Ant. 1 and Ant. 2 (Fig. 7(b)) is more than 25 dB in a wide bandwidth which confirms the significant improvement compared to the other works reported in [20], [28]. The simulated and measured reflection coefficients for mm-wave 5G band are shown in Fig. 8. The results show that the array (Port 3) operates at 28 GHz with -10 dB impedance matching bandwidth ranging from 25 GHz to 30 GHz. The measured isolation between low (Ant. 1) and high (Array) frequency ports as shown in Fig. 8 is more than 30 dB.

The far-field 2D normalized radiation patterns in the azimuth ($\phi = 0^o$) and elevation ($\theta = 90^o$) planes for Ant. 1

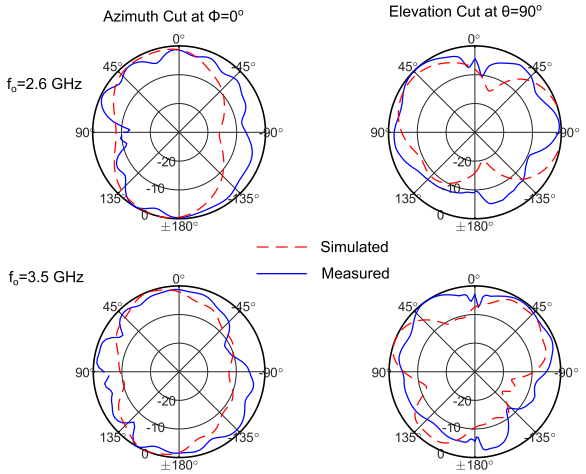

FIGURE 9. The simulated and measured 2D normalized radiation patterns for Ant. 1 at 2.6 GHz and 3.5 GHz.

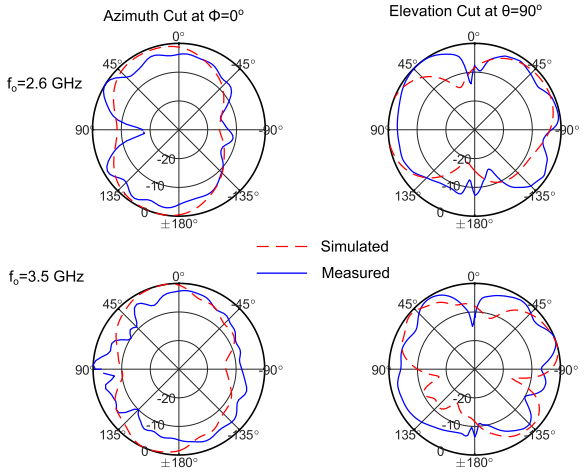

FIGURE 10. The simulated and measured 2D normalized radiation patterns for Ant. 2 at 2.6 GHz and 3.5 GHz.

and Ant. 2 at two different low frequencies, i.e. 2.6 GHz and 3.5 GHz are shown in Fig. 9 and Fig. 10, respectively. As expected, both antennas have omni-directional radiation patterns which can also be verified from the 3D simulated radiation patterns shown in Fig. 11. It can also be seen from 3D radiation patterns that both antennas have slightly tilted radiation patterns which help in providing diversity performance with low correlation. The simulated and measured efficiency curves are shown in Fig.13. A 4 dB measured realized gain and more than 85% measured efficiency is achieved for both antennas. A good agreement is observed in all simulated and measured results.

The far-field 2D radiation patterns in the azimuth ($\phi = 0^o$) and elevation ($\theta = 90^o$) planes for an array at two selected high frequencies, i.e. 26.5 GHz and 28 GHz, are shown in Fig. 12. The results show that the proposed array has end-fire directional patterns with low side-lobe levels. The realized gain and radiation efficiency curves are shown in Fig.13. A high gain of 15 dB is obtained at 5G band

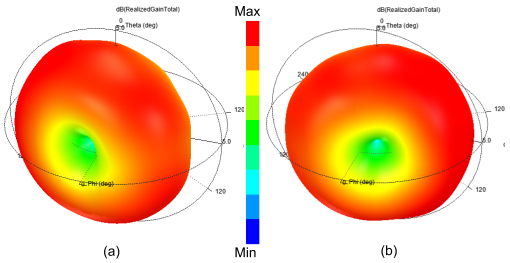

FIGURE 11. The simulated 3D radiation patterns for (a) Ant. 1 and (b) Ant. 2 at 2.6 GHz.

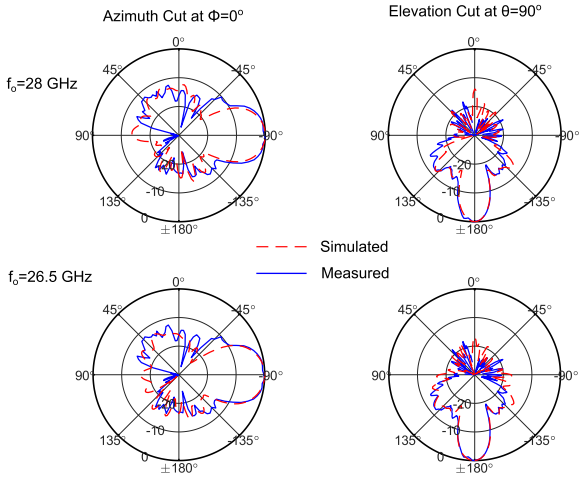

FIGURE 12. The simulated and measured 2D normalized radiation patterns for 5G array at 28 GHz and 26.5 GHz.

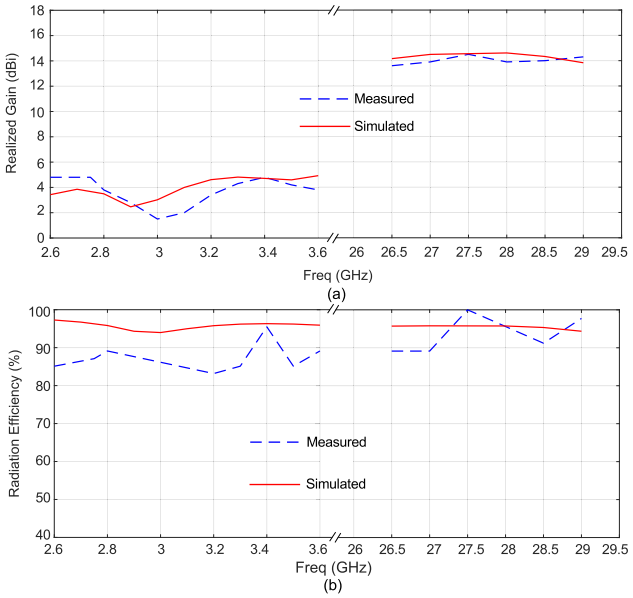

FIGURE 13. The simulated and measured (a) realized gain and (b) radiation efficiency for low and high frequency bands.

which in comparison is much higher than the other recently presented works for 4G/5G application [3], [4], [12], [13]. The measured radiation efficiency is more than 85 % in the 5G band from 26.5 GHz to 29 GHz.

TABLE 1. Comparison between the proposed and recently reported 4G/5G integrated antenna designs for mobile devices.

Figure of merits	**Proposed work**	[3]	[4]	[13]	[12]
Covered frequency bands	2.45-2.85 GHz 3.18-3.68 GHz 25-30 GHz	2.0-2.6 GHz 23-29 GHz	700-960 MHz 1.71-2.69 GHz 25-30 GHz	822-995 MHz 1.36-2.79 GHz 24.25-27.5 GHz	740-960 MHz 1.7-2.2 GHz 22-31 GHz
MIMO design at microwave band	Yes	Yes	No	No	No
Isolation at microwave band	25 dB	19	N/A	N/A	N/A
Realized Gain at mm-wave band	15 dBi	12.5 dBi	7.0 dBi	8.0 dBi	9.5 dBi

Finally, the MIMO performance of the proposed design in terms of Envelope Correlation Coefficient (ECC) and Diversity Gain (DG) is also computed. The ECC and DG are calculated using the following equations [27], [31].

$$\rho_e = \frac{|\int\int_0^{4\pi}[\vec{F}_1(\theta,\phi)\times\vec{F}_2(\theta,\phi)]d\Omega|^2}{\int\int_0^{4\pi}|\vec{F}_1(\theta,\phi)|^2 d\Omega \int\int_0^{4\pi}|\vec{F}_2(\theta,\phi)|^2 d\Omega} \quad (1)$$

where, ρ_e is the ECC, $\vec{F}_1(\theta,\phi)$ and $\vec{F}_2(\theta,\phi)$ are the 3D radiation patterns of Ant. 1 and Ant. 2, respectively, while Ω is the solid angle.

$$DG = 10\sqrt{1-|ECC|^2} \quad (2)$$

where, DG is the diversity gain.

According to (1), the ECC values, before adding the decoupling structure, between Ant. 1 and Ant. 2 are 0.053 and 0.011 at 2.6 GHz and 3.5 GHz, respectively. The values of ECC, after adding the decoupling structure, are reduced to 0.024 and 0.0068, whereas the values of DG are 9.997 and 9.999, which is desirable for MIMO applications. The results are expected as improving isolation lowers ECC values.

Table 1 summaries the significance of the proposed work compared to the other reported 4G/5G integrated designs. It is found that the proposed design supports MIMO operation at microwave band, while others do not except [3]. The achieved isolation between MIMO antennas is more than 25 dB which is 6 dB higher than the design demonstrated in [3]. Additionally, the proposed array provides a realized gain of 15 dBi at mm-wave bands which is significantly high compared to the other designs.

V. CONCLUSION

An integrated antenna design employing dual-functional tapered slot antenna array has been presented for 4G/5G applications. The proposed design consists of 2-element Multiple-Input Multiple-Output (MIMO) antenna system working at microwave bands. Then, a tapered slot antenna array (TSAA) is added to the design to work as a decoupling structure at microwave frequencies and as an antenna array at mm-wave frequency. The TSAA provides 1.2 GHz isolation bandwidth from 2.45 GHz to 3.65 GHz, while working as a decoupling structure and 5 GHz impedance matching bandwidth from 25 GHz to 30 GHz, while working as an antenna array with 15 dBi of realized gain. More than 25 dB isolation is achieved at both low and high frequency bands.

REFERENCES

[1] W. Hong, "Solving the 5G mobile antenna puzzle: Assessing future directions for the 5G mobile antenna paradigm shift," *IEEE Microw. Mag.*, vol. 18, no. 7, pp. 86–102, Nov. 2017.

[2] N. Shoaib, S. Shoaib, R. Y. Khattak, I. Shoaib, X. Chen, and A. Perwaiz, "MIMO antennas for smart 5G devices," *IEEE Access*, vol. 6, pp. 77014–77021, 2018.

[3] M. Ikram, E. A. Abbas, N. Nguyen-Trong, K. H. Sayidmarie, and A. Abbosh, "Integrated frequency-reconfigurable slot antenna and connected slot antenna array for 4G and 5G mobile handsets," *IEEE Trans. Antennas Propag.*, to be published.

[4] J. Kurvinen, H. Kähkönen, A. Lehtovuori, J. Ala-Laurinaho, and V. Viikari, "Co-designed mm-wave and LTE handset antennas," *IEEE Trans. Antennas Propag.*, vol. 67, no. 3, pp. 1545–1553, Mar. 2019.

[5] L. Zhang, K. Y. See, B. Zhang, and Y. P. Zhang, "Integration of dual-band monopole and microstrip grid array for single-chip tri-band application," *IEEE Trans. Antennas Propag.*, vol. 61, no. 1, pp. 439–443, Jan. 2013.

[6] M.-Y. Li, Y.-L. Ban, Z.-Q. Xu, J. Guo, and Z.-F. Yu, "Tri-polarized 12-antenna MIMO array for future 5G smartphone applications," *IEEE Access*, vol. 6, pp. 6160–6170, 2017.

[7] Y. Li, C.-Y.-D. Sim, Y. Luo, and G. Yang, "Multiband 10-antenna array for sub-6 GHz MIMO applications in 5-G smartphones," *IEEE Access*, vol. 6, pp. 28041–28053, 2018.

[8] M. S. Sharawi, M. Ikram, and A. Shamim, "A two concentric slot loop based connected array MIMO antenna system for 4G/5G terminals," *IEEE Trans. Antennas Propag.*, vol. 65, no. 12, pp. 6679–6686, Dec. 2017.

[9] Q. Chen, H. Lin, J. Wang, L. Ge, Y. Li, T. Pei, and C.-Y.-D. Sim, "Single ring slot-based antennas for metal-rimmed 4G/5G smartphones," *IEEE Trans. Antennas Propag.*, vol. 67, no. 3, pp. 1476–1487, Mar. 2019.

[10] A. Zhao and Z. Ren, "Wideband MIMO antenna systems based on coupled-loop antenna for 5G N77/N78/N79 applications in mobile terminals," *IEEE Access*, vol. 7, pp. 93761–93771, 2019.

[11] N. O. Parchin, Y. I. A. Al-Yasir, A. H. Ali, I. Elfergani, J. M. Noras, J. Rodriguez, and R. A. Abd-Alhameed, "Eight-element dual-polarized MIMO slot antenna system for 5G smartphone applications," *IEEE Access*, vol. 7, pp. 15612–15622, 2019.

[12] M. M. S. Taheri, A. Abdipour, S. Zhang, and G. F. Pedersen, "Integrated millimeter-wave wideband end-fire 5G beam steerable array and low-frequency 4G LTE antenna in mobile terminals," *IEEE Trans. Veh. Technol.*, vol. 68, no. 4, pp. 4042–4046, Apr. 2019.

[13] R. Rodriguez-Cano, S. Zhang, K. Zhao, and G. F. Pedersen, "Reduction of main beam-blockage in an integrated 5G array with a metal-frame antenna," *IEEE Trans. Antennas Propag.*, vol. 67, no. 5, pp. 3161–3170, May 2019.

[14] T. Zhihong, Y. P. Zhang, C. Luxey, A. Bisognin, D. Titz, and F. Ferrero, "A ceramic antenna for tri-band radio devices," *IEEE Trans. Antennas Propag.*, vol. 61, no. 11, pp. 5776–5780, Nov. 2013.

[15] D. Wang and C. H. Chan, "Multiband antenna for WiFi and WiGig communications," *IEEE Antennas Wireless Propag. Lett.*, vol. 15, pp. 309–312, 2016.

[16] S. I. Naqvi, A. H. Naqvi, F. Arshad, M. A. Riaz, M. A. Azam, M. S. Khan, Y. Amin, J. Loo, and H. Tenhunen, "An integrated antenna system for 4G and millimeter-Wave 5G future handheld devices," *IEEE Access*, vol. 7, pp. 116555–116566, 2019.

[17] R. Hussain, M. U. Khan, and M. S. Sharawi, "An integrated dual MIMO antenna system with dual-function GND-plane frequency-agile antenna," *IEEE Antennas Wireless Propag. Lett.*, vol. 17, pp. 142–145, 2018.

[18] M. Ikram, R. Hussain, and M. S. Sharawi, "4G/5G antenna system with dual function planar connected array," *IET Microw., Antennas Propag.*, vol. 11, no. 12, pp. 1760–1764, 2017.
[19] M. Ikram, M. S. Sharawi, A. Shamim, and A. Sebak, "A multiband dual-standard MIMO antenna system based on monopoles (4G) and connected slots (5G) for future smart phones," *Microw. Opt. Technol. Lett.*, vol. 60, no. 6, pp. 1468–1476, 2018.
[20] M. Ikram, N. Nguyen-Trong, and A. Abbosh, "Multiband MIMO microwave and millimeter antenna system employing dual-function tapered slot structure," *IEEE Trans. Antennas Propag.*, vol. 67, no. 8, pp. 5705–5710, Aug. 2019.
[21] C.-Y. Chiu, C.-H. Cheng, R. D. Murch, and C. R. Rowell, "Reduction of mutual coupling between closely-packed antenna elements," *IEEE Trans. Antennas Propag.*, vol. 55, no. 6, pp. 1732–1738, Jun. 2007.
[22] Q. Cai, Y. Li, X. Zhang, and W. Shen, "Wideband MIMO antenna array covering 3.3–7.1 GHz for 5G metal-rimmed smartphone applications," *IEEE Access*, vol. 7, pp. 142070–142084, 2019.
[23] J. Li, X. Zhang, Z. Wang, X. Chen, J. Chen, Y. Li, and A. Zhang, "Dual-band eight-antenna array design for MIMO applications in 5G mobile terminals," *IEEE Access*, vol. 7, pp. 71636–71644, 2019.
[24] A. T. Alreshaid, R. Hussain, S. K. Podilchak, and M. S. Sharawi, "A dual-element MIMO antenna system with a mm-Wave antenna array," in *Proc. 10th Eur. Conf. Antennas Propag. (EuCAP)*, Apr. 2016, pp. 1–4.
[25] F. Yang and Y. Rahmat-Samii, "Microstrip antennas integrated with electromagnetic band-gap (EBG) structures: A low mutual coupling design for array applications," *IEEE Trans. Antennas Propag.*, vol. 51, no. 10, pp. 2936–2946, Oct. 2003.
[26] S. Zhang and G. F. Pedersen, "Mutual coupling reduction for UWB MIMO antennas with a wideband neutralization line," *IEEE Antennas Wireless Propag. Lett.*, vol. 15, pp. 166–169, 2016.
[27] A. A. Ghannad, M. Khalily, P. Xiao, R. Tafazolli, and A. A. Kishk, "Enhanced matching and vialess decoupling of nearby patch antennas for MIMO system," *IEEE Antennas Wireless Propag. Lett.*, vol. 18, no. 6, pp. 1066–1070, Jun. 2019.
[28] S. Tebache, A. Belouchrani, F. Ghanem, and A. Mansoul, "Novel reliable and practical decoupling mechanism for strongly coupled antenna arrays," *IEEE Trans. Antennas Propag.*, vol. 67, no. 9, pp. 5892–5899, Sep. 2019.
[29] P. J. Gibson, "The Vivaldi aerial," in *Proc. 9th Eur. Microw. Conf.*, Sep. 1979, pp. 101–105.
[30] K. Ebnabbasi, D. Busuioc, R. Birken, and M. Wang, "Taper design of Vivaldi and co-planar tapered slot antenna (TSA) by Chebyshev transformer," *IEEE Trans. Antennas Propag.*, vol. 60, no. 5, pp. 2252–2259, May 2012.
[31] M. S. Sharawi, *Printed MIMO Antenna Engineering*. Norwood, MA, USA: Artech House, 2014.

MUHAMMAD IKRAM (S'19) received the B.Sc. and M.Sc. degrees in electrical engineering from the University of the Punjab, Pakistan, and the King Fahd University of Petroleum and Minerals (KFUPM), Saudi Arabia, in 2014 and 2017, respectively. He is currently pursuing the Ph.D. degree in electrical engineering with the School of ITEE, The University of Queensland (UQ), Australia. He is also a member of the Electromagnetic Innovations (εMAGin) Group at UQ. His current research interests include integrated MIMO antenna designs for 4G/5G mobile handsets and future wireless devices, antenna arrays, frequency and polarization reconfigurable antenna arrays, and mobile communications. He serves as a Reviewer of the IEEE TRANSACTIONS ON ANTENNAS AND PROPAGATION, IEEE ANTENNAS AND WIRELESS PROPAGATION LETTER, and IEEE ACCESS.

NGHIA NGUYEN-TRONG (M'17) received the Ph.D. degree in electrical engineering from The University of Adelaide, Adelaide, SA, Australia, in 2017. He is currently a Postdoctoral Research Fellow with The University of Queensland, Brisbane, QLD, Australia. His current research interests include leaky-wave antennas, monopolar antennas, Fabry-Perot antennas, and reconfigurable antennas. He was a recipient of the Best Student Paper Award at the 2014 IWAT, 2015 IEEE MTT-S NEMO, and 2017 ASA Conferences, and the Best Paper Award at 2018 AMS Conference. He was selected as Top Reviewer for the IEEE TRANSACTIONS ON ANTENNA AND PROPAGATION and the IEEE ANTENNA WIRELESS AND PROPAGATION LETTER, in 2018.

AMIN M. ABBOSH (SM'08) received the Doctor of Engineering degree from the University of Queensland, in 2013. He leads the Electromagnetic Innovations (εMAGin) Group and is the Head of the School of Information Technology and Electrical Engineering, The University of Queensland, Australia. He has authored more than 400 articles on electromagnetic imaging systems for medical applications, wideband passive microwave devices, and planar antennas. He is an Associate Editor for the IEEE TRANSACTIONS ON ANTENNAS AND PROPAGATION and the Senior Associate Editor for the IEEE ANTENNAS AND WIRELESS PROPAGATION LETTERS.